ACS APPLIED MATERIALS & INTERFACES

Research Article

www.acsami.org

In Situ Raman Spectroscopy of Sulfur Speciation in Lithium−Sulfur Batteries

Heng-Liang Wu, Laura A. Huff, and Andrew A. Gewirth*

Department of Chemistry, University of Illinois at Urbana−Champaign, 600 South Mathews Avenue, Urbana, Illinois 61801, United States

Supporting Information

ABSTRACT: In situ Raman spectroscopy and cyclic voltammetry were used to investigate the mechanism of sulfur reduction in lithium−sulfur battery slurry cathodes with 1 M lithium bis(trifluoromethane sulfonyl)imide (LiTFSI) and tetraethylene glycol dimethyl ether (TEGDME)/1,3-dioxolane (DIOX) (1/1, v/v). Raman spectroscopy shows that long-chain polysulfides (S_8^{2-}) were formed via S_8 ring opening in the first reduction process at ∼2.4 V vs Li/Li^+ and short-chain polysulfides such as S_4^{2-}, S_4^-, $S_3^{\bullet-}$, and $S_2O_4^{2-}$ were observed with continued discharge at ∼2.3 V vs Li/Li^+ in the second reduction process. Elemental sulfur can be reformed in the end of the charge process. Rate constants obtained for the appearance and disappearance polysulfide species shows that short-chain polysulfides are directly formed from S_8 decomposition. The rate constants for S_8 reappearance and polysulfide disappearance on charge were likewise similar. The formation of polysulfide mixtures at partial discharge was found to be quite stable. The CS_2 additive was found to inhibit the sulfur reduction mechanism allowing the formation of long-chain polysulfides during discharge only and stabilizing the S_8^{2-} product.

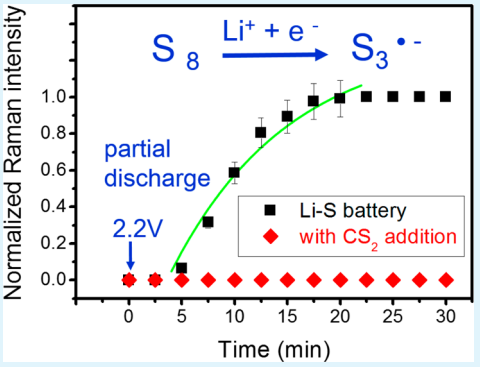

KEYWORDS: *Li−S batteries, Raman spectroscopy, sulfur reduction, kinetic of polysulfides formation and decomposition, partial discharge, carbon disulfide*

1. INTRODUCTION

Conventional Li-ion batteries have attracted attention over the previous two decades for a wide variety of applications, including those involving portable devices and automobiles. However, the gravimetric energy density limit for the $LiCoO_2$/C battery is about 400 Wh kg^{-1}, which is insufficient for long distance travel (i.e., >300 km) involving battery electric vehicles.[1,2] The lithium−sulfur (Li−S) battery is a promising electrochemical system that has great potential as a higher capacity energy storage device. The theoretical capacity of the Li−S battery is 1675 mAh g^{-1} and the energy density of 2600 Wh kg^{-1} is 3−5 fold higher than state-of-the-art Li-ion batteries. Additionally, the volumetric energy density of the Li−S battery is theoretically two times larger than that associated with the Li-ion battery, 2200 Wh L^{-1} vs 1000 Wh L^{-1}, respectively.[1] Finally, elemental sulfur is safe, abundant, cheap, and nontoxic.

Despite the considerable advantages of the Li−S battery, it suffers from many challenges such as the formation of solid electrolytes interphase (SEI) layers on the Li anodes, Li dendrite formation, the shuttle effect of polysulfides, dissolution of partially discharged species, and a complicated reaction pathway.[1−5]

Sulfur reduction is a stepwise electrochemical process involving a sequence of highly soluble polysulfides as the intermediate species. It is generally agreed that long-chain polysulfides with the general formula (Li_2S_n) such as Li_2S_8 and Li_2S_6 are produced in the beginning of the discharge process. The long-chain polysulfides are further reduced to form short-chain polysulfides, the dissolution of which is well-understood to cause capacity fade. The final product at the end of discharge is insoluble lithium sulfide (Li_2S).[1−5] The overall cathode reaction can be described as $S_8 + 16e^- + 16Li^+ \leftrightarrow 8Li_2S$.

To understand the discharge/charge mechanism of the Li−S battery, sulfur speciation has been examined by multiple techniques.[6−13] UV−visible absorption spectroscopy (UV−vis) and cyclic voltammetry (CV) were used to study the dissolved lithium polysulfides produced from the electrochemical reduction of S_8. The electrochemical reduction of S_8 normally exhibits two reduction steps in ionic liquids and organic solvents such as tetrahydrofuran (THF), dimethylformamide (DMF) and dimethyl sulfoxide (DMSO).[14−20] In some reports, there is an additional peak in the CV exhibiting smaller reduction current between the two main reduction peaks at ∼2.1 V (vs Li/Li^+).[8,14−16,18,19] Long-chain polysulfides such as S_8^{2-} and S_6^{2-} are produced in the first reduction step, as evidenced in UV−vis and high-performance liquid chromatography. S_4^{2-} is produced in the second reduction peak. Short-chain polysulfides such as S_3^{2-}, S_2^{2-}, and S^{2-} are produced at the end of the reduction process.[8]

Received: October 21, 2014
Accepted: December 26, 2014
Published: December 26, 2014

DOI: 10.1021/am5072942
ACS Appl. Mater. Interfaces 2015, 7, 1709−1719

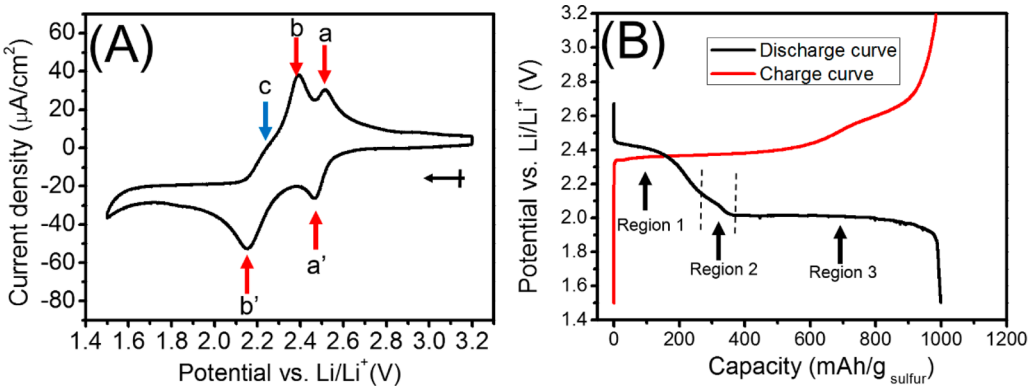

Figure 1. (A) Steady cyclic voltammetry of the as-prepared sulfur−carbon cathode at a scan rate of 1 mV/s. (B) Li−S battery discharge and charge curve (chronopotentiometric) at a C/10 rate (for the weight of whole cathode).

X-ray absorption spectroscopy showed that the sulfur speciation in the Li−S battery during the discharge/charge process governs the dissolution of S_8 and deposition of Li_2S.[10] This study also suggested that supersaturation of S^{2-} postpones the Li_2S formation upon reduction. Solid-state ^6Li and ^{33}S magic-angle spinning NMR studies demonstrated that Li_2S is produced at the end of the discharge process. ^6Li T_2 relaxation measurements show the association of long-chain polysulfides and short-chain polysulfides with two reduction steps.[21] In situ X-ray diffraction characterization shows the formation of crystalline Li_2S in the discharge process and its consumption during following charge process. The soluble polysulfides can be oxidized to solid S_8. After the recrystallization process, the reformed S_8 is a different allotrope from the pristine structure.[12]

In this paper, we use in situ Raman spectroscopy to examine the discharge and charge processes of a Li−S cathode in 1 M lithium bis(trifluoromethane sulfonyl)imide (LiTFSI) and tetraethylene glycol dimethyl ether (TEGDME)/1,3-dioxolane (DIOX) (1/1, v/v). There has been substantial prior work using Raman to interrogate sulfur speciation.[6,7,22] Hagen et al. combined DFT calculations and in situ Raman experiments to verify the existence of various polysulfides, whose speciation depends on the state of charge. They found both polysulfide monoanions and dianions in every charge state.[7] Yeon et al. showed that the radical anion $S_3^{\bullet-}$ and Li_2S were formed in a sulfur−carbon cathode during cycling by using ex situ Raman spectroscopy.[6] However, detailed examination of the potential dependence of particular polysulfide species and in particular the rates of disappearance and appearance of sulfur speciation are not yet clear. Additionally, the effect of solution additives on intermediate species is still unknown. Thus, we aim to provide more detailed information for the potential dependence of different polysulfide species and the rates of formation for sulfur species during the discharge and charge processes along with the effect of additives such as CS_2. In prior work, addition of S copolymers such as poly(sulfur-1,3-diisopropenylbenzene) has been shown to control S_8 discharge.[23] CS_2 has been utilized to increase the solubility of elemental S and the increased solubility of this element is thought to increase the charge−discharge efficiency.[24] However, the detailed effect of CS_2 on the voltammetry or S speciation is unknown.

2. EXPERIMENTAL SECTION

Cathode Preparation. The cathode materials were made from a slurry consisting of 60 wt % sulfur (99.98%, Sigma-Aldrich), 30 wt % carbon black (Super-P Li, Timcal Inc.), and 10 wt % polyvinylidene fluoride (PVDF, Kynar 2801) binder mixed with anhydrous *N*-methyl-2-pyrrolidone (NMP, Sigma-Aldrich). After mixing the slurry overnight, the slurry was cast on aluminum foil (Sigma-Aldrich). A Gardco adjustable micrometer film applicator (Microm 5 1/2″ width) was used to smooth the slurry film. The slurry film was then dried in a convection oven overnight at 55 °C.

Two-Electrode Coin-Cell Preparation and Performance. Lithium−sulfur batteries were assembled in a modified Swagelok tube fitting apparatus (nylon, 1/2″ inner diameter, Chicago Fluid System Technologies) described previously.[21] The cell consisted of a Li metal (99.9%, Alfa Aesar) anode, a porous polypropylene separator (Celgard 2400), Whatman glass fiber separator (GF/F, 150 mm diameter) and carbon cathode to which about 0.3 mL of electrolyte was added. The cells were assembled and discharge/charge curves were obtained in an Ar-filled glovebox. Discharge and charge studies were carried out at the rate of C/10 (by the weight of the whole cathode) from the open circuit potential (OCP) to 1.5 V. All materials were handled in an Ar-filled glovebox unless otherwise stated.

Cyclic Voltammetry (CV) and Raman Cell Preparation. CV and Raman spectroscopy experiments were performed in a home-built glass cell.[25] The working electrode was sulfur−carbon (~0.01g) supported on an Al disk (3/8 in. in diameter, 99.99%, Alfa Aesar). Li metal was used as the reference and counter electrode (99.9%, Alfa Aesar). The assembled cell was filled with 20 mL electrolyte in an Ar-filled glovebox and then transferred out of glovebox for in situ Raman experiments. The sulfur concentration in our Raman study is ~9 mM.

Cyclic voltammetry and discharge/charge performance of the cells were carried out in the potential window from 3.2 to 1.5 V (vs Li/Li^+), using 760C and 760D CH Instruments potentiostat. The scan rates were 0.5 mV/s. The current density was estimated by using the geometric area of the Al disk.

Electrolyte Preparation. The electrolyte was 1 M lithium bis(trifluoromethane sulfonyl)imide (LiTFSI) in a 1:1 (v/v) solution of tetraethylene glycol dimethyl ether (TEGDME, ≥99%, Sigma-Aldrich) and 1,3-dioxolane (DIOX, anhydrous, Sigma-Aldrich). The carbon disulfide (CS_2) additive was purchased from Sigma-Aldrich (anhydrous, ≥99.9%).

Raman Spectroscopy Measurements. Raman spectroscopy was performed using a system described previously.[25] The typical acquisition time was 75s or 150s per spectrum. In order to reach electrochemical equilibrium, the potential was held at each 100 mV step at least 15 min before collecting the spectrum. The band intensities used for the data analysis in this study were baseline corrected. The error bars in the Raman intensity were obtained from five experiments. The magnitude of the error bars shows the error in the average Raman intensity. The analysis in our experimental system is valid.

3. RESULTS AND DISCUSSION

3.1. Cyclic Voltammetry and Discharge/Charge Profiles for Sulfur−carbon Cathode. Figure 1A shows the

DOI: 10.1021/am5072942
ACS Appl. Mater. Interfaces 2015, 7, 1709−1719

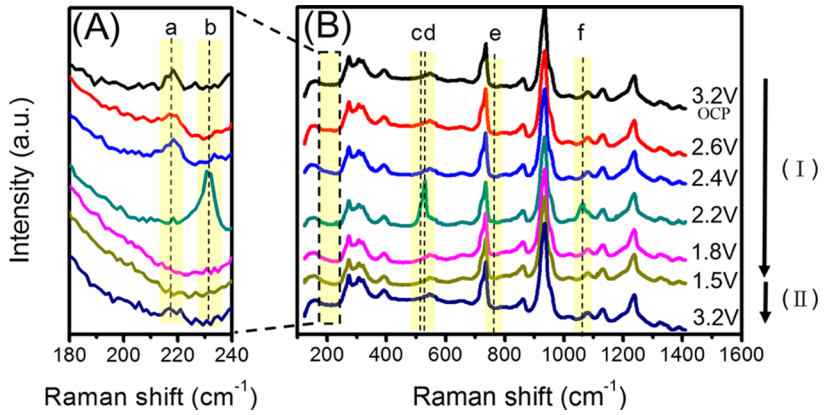

Figure 2. (A, B) In situ Raman spectra of the sulfur−carbon cathode shown at representative potentials (I) during discharge from 3.2 to 1.5 V and after (II) recharging to 3.2 V.

steady cyclic voltammetry (CV) of the as-prepared sulfur−carbon cathodes obtained at a scan rate of 0.5 mV/s. The CV starts from the open circuit potential (3.2 V) to 1.5 V vs Li/Li^+. The reductive scan shows typical sulfur-reducing CV peaks at ∼2.45 and ∼2.20 V as marked by a′ and b′, respectively. These reduction processes are associated with the formation of various polysulfides.[8,14,15,17−20]

Barchasz et al. showed that the CV of as-prepared sulfur−carbon cathodes contains three redox pairs at a scan rate of 20 μV/s. The three reductive peaks only appear in the first cycle at ∼2.4 V, ∼2.1 V and ∼2 V (vs Li/Li^+). However, the second reductive peak at ∼2.1 V only appears at specific scan rates and cycle numbers because the intermediate species produced during the first cycle is unstable.

Peak a′ is associated with the formation of long-chain polysulfides as a consequence of opening the S_8 ring. These polysulfide chains are then shortened as sulfur is further reduced in the second reduction peak (peak b′) leading ultimately to the formation of Li_2S at ca. 1.9 V. In the anodic scan from 1.5 to 3.2 V, there are three oxidative peaks at ∼2.52 V (a) and ∼2.38 V (b) with a small shoulder at ∼2.25 V (c). These oxidation processes are associated with the oxidation of polysulfides to elemental sulfur. The presence of three oxidation peaks suggests that there should be three corresponding reduction peaks. Indeed, in the reductive scan, peak (b′) is broad than peak (a′), which suggest that there are multiple peaks overlapping. The broad reduction peak at 2.15 V could be attributed to the peak overlap. The potential of the second reduction peak (2.15 V) in the CV is slightly different relative to that found in a coin cell (2.0 V) with a scan rate of 20 μ V/s as shown in the Supporting Information (Figure S1) and reported previously.[8] The more anodic potential of the second reduction peak in the CV may due to the higher lithium availability relative to the coin cell in which inhibition of the formation of smaller, lithiated polysulfides may occur.

Figure 1B shows a typical discharge and charge curve obtained from a lithium−sulfur (Li−S) battery at a rate of C/10. In the first discharge process, the capacity ranging from 800 to 1200 mAh/g is similar to that reported previously.[2,4,13] The reduction process of Li/S battery can be divided into three regions based on the discharge profile (labeled as regions 1, 2, and 3) which provides further support for the existence of three reductive peaks in the CV. The charge profile shows the plateaus around ∼2.35 V and ∼2.58 V, which associated with the oxidation peaks in the CV. Our discharge and charge profiles are in a good agreement with Barchasz et al. and Cuisinier et al.[8,10] The identity of the three processes associated with the three regions of the discharge curve has been studied using many techniques such as XPS,[13] Raman,[6,7] UV−visible spectra,[8,9] X-ray absorption spectroscop, and XRD measurements.[10−12] Region 1 is associated with the formation of long-chain polysulfides such as S_8^{2-} and S_6^{2-} via S−S bond cleavage by Li^+. Regions 2 and 3 are associated with the formation of short-chain polysulfides such as S_4^{2-} and S_3^{2-}. The short polysulfide species like S^{2-} and S_2^{2-} along with Li_2S are the final products at the end of region 3.[6−13]

3.2. Raman Intensity Changes during Discharge. To fully understand the mechanism of polysulfide formation during charge and discharge, we used in situ Raman spectroscopy to investigate the potential dependence of these polysulfide species. Figure 2 shows in situ Raman spectra obtained from the sulfur−carbon cathode during discharge from 3.2 to 1.5 V (I) followed by recharge to 3.2 V (II). The peaks of particular interest are marked with a−f. Raman spectra of solid-state polysulfides and solvated polysulfides in different solvents have been previously reported.[6,7,22,26−39] It is known that the vibrational frequency of different polysulfides is solvent dependent. Values obtained from DFT calculations were also taken into account in the assignment given here.[7] Polysulfide modes are found between 100 and 800 cm^{-1} and are associated with S−S bending and stretching vibrations, as shown in Table 1. The other peaks can be ascribed to the electrolyte and are discussed in the Supporting Information (Figure S2 and Table S1)

Peak a at 217 cm^{-1} is observed at positive potentials prior to cycling the electrode. This peak disappears during the discharge process and reforms during charging as shown in Figure 2. Peak

Table 1. Experimental Vibrational Frequencies and Assignments for Li−S Species

peak label	peak position (cm^{-1})	assignments	literature references
a	217	S_8 and S_8^{2-} (Bending mode)	6,7,26,27,40,41
b	234	S_4^{2-}(Bending mode)	34,35,37
c	518	S_4^-	36,38
d	534	$S_3^{\cdot-}$ (Symmetric stretching mode)	6,42,43
e	766	S_x^{2-} (X=4−8)	6,28
f	1066	$S_2O_4^{2-}$ (S−O, stretching mode)	22,46,47

DOI: 10.1021/am5072942
ACS Appl. Mater. Interfaces 2015, 7, 1709−1719

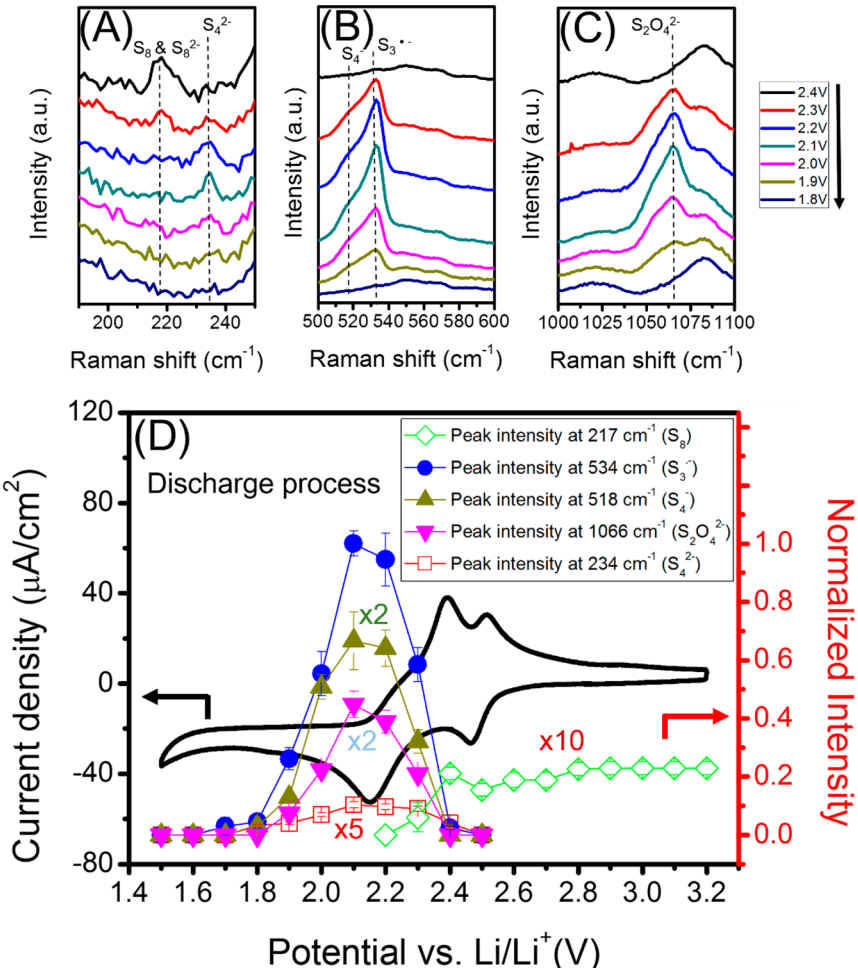

Figure 3. In situ Raman spectra of the sulfur−carbon cathode obtained during discharge at (A) 180−250 cm^{-1}, (B) 500−600 cm^{-1}, and (C) 1000−1100 cm^{-1} from 2.4 to 1.5 V. (D) Cyclic voltammetry of the as-prepared sulfur−carbon cathode and potential dependence of the peak intensities at 217, 234, 518, 534, and 1066 cm^{-1} shown in A−C.

a is assigned to the S−S bending mode of S_8 ring.[6,26,27,40,41] The Raman spectra suggest that the S_8 ring reversibly is destroyed and reformed during cycling, a result also suggested by XRD results.[6,11,12] The peaks at 234 cm^{-1} (b), 518 cm^{-1} (c), 534 cm^{-1} (d), 766 cm^{-1} (e), and 1066 cm^{-1} (f) gradually grow in at 2.2 V during discharge. Peak b is assigned to bending mode of S_4^{2-}.[34,35,37] Peak c is S_4^{-} and peak d is attributed to radical anion $S_3^{\bullet-}$ which has been found by prior Raman measurements at 535 cm^{-1}.[6,36,38,42,43] The existence of a radical anion is also suggested by UV−visible spectra and ESR measurements.[42−45] Interestingly, $S_3^{\bullet-}$ has also been found in ex situ Raman measurements obtained from a disassembled Li−S battery, suggesting it is quite stable.[6] Peak (e) was assigned to S_x^{2-} (x = 4−8) which was reported for long polysulfides solutions such as Li_2S_5, Li_2S_6, and $Li_2S_{6.5}$ and was also observed by ex situ Raman experiment.[6,28] The presence of $S_2O_4^{2-}$ at peak (f) shows evidence of S−O species formation during discharge.[46,47] The preparation of sulfur−carbon cathode outside of the glovebox may result in the formation of sulfur−oxygen species. Another possibility may be the presence of a small amount of oxygen (3−7 ppm) in the glovebox. Recently, irreversible sulfur oxidation process on the sulfur−carbon cathode has been reported.[22,48] In this work, the reaction between the sulfur−carbon electrode and solvent (TEGDME/1,3-dioxolane) could be another reason causing the formation of S−O species.

The different short-chain polysulfides such as S_4^{2-}, S_4^{-}, and $S_3^{\bullet-}$ can be formed at the same potential. The polysulfide species could result of the reaction of $S_8+2e^- \rightarrow S_8^{2-}$, $2S_8^{2-} \rightarrow 2S_4^{2-}+S_8$, and $2S_4^{2-} \rightarrow 2S_3^{\bullet-}+S_2^{2-}$.[8,28] The presence of $S_3^{\bullet-}$ suggest the equilibrium of $Li_2S_4 \rightarrow Li_2S$. It is known that the crystalline and partially disordered Li_2S phase can be formed in the end of discharge process by using XPS,[13] X-ray absorption spectroscopy,[10] solid-state NMR, and XRD measurements.[6,11,12,21] One peak not observed in the Raman in Figure 2 is that associated with Li_2S, the final product of battery discharge, even when the cathode was held at 1.5 V at least 20 min. Solid Li_2S exhibits a peak at 375 cm^{-1},[49] but solvent modes obscure this energy in our in situ measurement. Additionally, ex situ Raman from discharged Li−S cathodes revealed little intensity at this energy.[6] Additional peaks at 174 and 514 cm^{-1} are for crystalline Li_2S_2.[22] In our in situ Raman experiment, the peak at ∼518 cm^{-1} showed up during discharge and disappear around 1.8 V as shown in Figure 2. It should be questioned whether the peak at 514 cm^{-1} is the pure Li_2S_2 or different polysulfides. Hagen et al. combined the DFT calculation and in situ Raman experiment to discuss the Li_2S_2 and Li_2S formation.[7] The experimental solid-state spectra were also taken into consideration. In summary, the intensity of the

DOI: 10.1021/am5072942
ACS Appl. Mater. Interfaces 2015, 7, 1709−1719

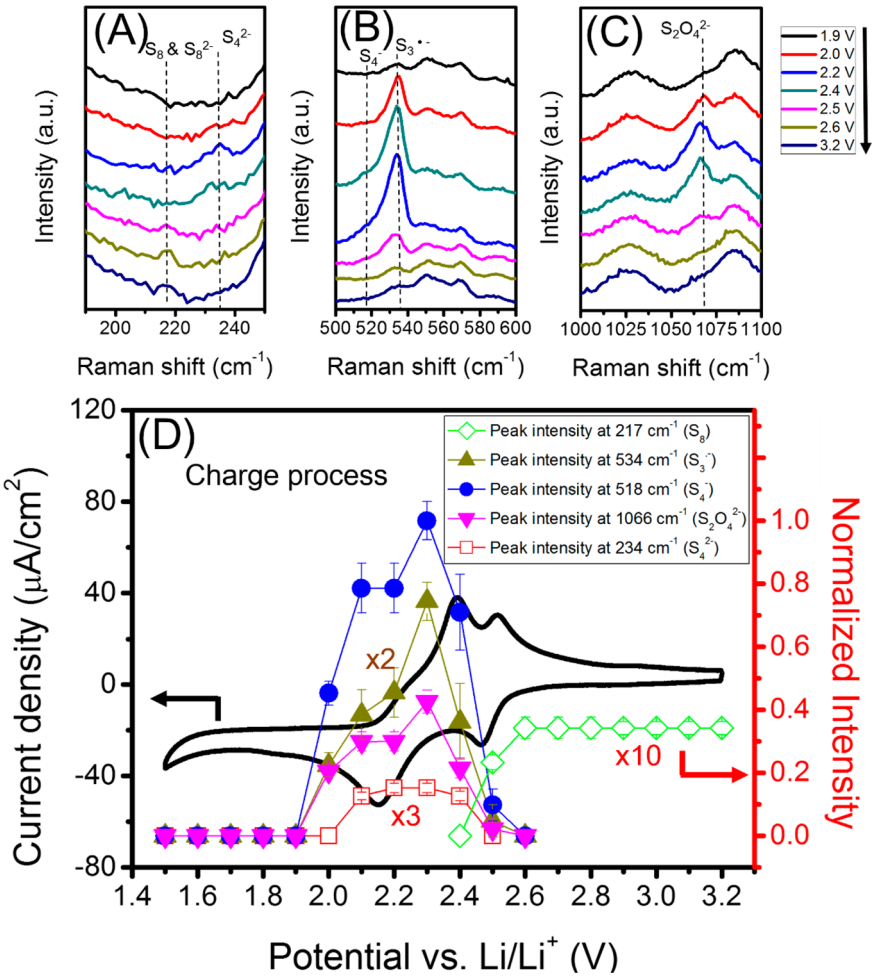

Figure 4. In situ Raman spectra of the sulfur−carbon cathode obtained during charging at (A) 180−250, (B) 500−600, and (C) 1000−1100 cm^{-1} from 1.5 to 3.2 V. (D) Cyclic voltammetry of the as-prepared sulfur−carbon cathode and potential dependence of the peak intensities at 217, 234, 518, 534, and 1066 cm^{-1} shown in A−C.

Li_2S_2 and Li_2S peaks is low and hard to identify as shown in the previous ex-situ and in situ Raman experiment.[6,7,22]

Figure 3A−C shows the potential dependence of the in situ Raman in three different spectral regions. Several new peaks form after the decomposition of long-chain polysulfide with further discharge below 2.4 V. Figure 3A−C shows that peaks associated with S_8 disappear at 2.2 V. S_4^{2-}, S_4^-, $S_3^{\bullet-}$, and $S_2O_4^{2-}$ grow around 2.3 V during the discharge and disappear at ∼1.6 V. Figure 3D presents the CV of the sulfur−carbon cathode and the potential dependence of the peak intensity at 217, 234, 518, 534, and 1066 cm^{-1} taken from Figure 3A−C. All peak intensities were normalized to the intense 534 cm^{-1} peak at 2.1 V. The S_8-associated peak at 217 cm^{-1} is present at 3.2 V and maintains approximately constant intensity until a potential of 2.2 V is reached, at which point the S_8-associated intensity drops to zero. The potential dependence in Figure 3D shows that intensity associated with S_8 decreases at approximately the potential of the first reduction peak upon discharge. Modest increases in intensity between 2.5 and 2.4 V may be associated with formation of species exhibiting a similar Raman shift relative to solid S_8. In particular, species such as mono- and dianions like S_5^- (217 cm^{-1}), S_8^- (216 cm^{-1}), S_5^{2-} (214 cm^{-1}), and S_8^{2-} (214 cm^{-1}) are calculated to exhibit similar shifts.[7] Indeed, S_8^{2-} or S_6^{2-} formation in this region has been suggested by using other techniques.[8,10,20] Figure 3D also presents the potential dependence of the peak intensities associated with S_4^-, S_4^{2-}, $S_3^{\bullet-}$, and $S_2O_4^{2-}$. These different polysulfide species all form at 2.3 V and grow to a maximum at ∼2.1 V. The coexistence of peaks associated with S_8 and S_4^{2-} can be observed at 2.3 V as shown in Figure 3A, suggesting that long-chain polysulfides are reduced to make shorter chains. This result clearly shows that the different short-chain polysulfides form at the second reductive peak in the CV and decompose into other species again at 1.8 V. Based on previous studies,[6,10,13,22] Li_2S and Li_2S_2 could be the final product but the solid Li_2S peak at 375 cm^{-1} was not observed as described above.

3.3. Raman Intensity Changes during Charging. Figure 4A−C shows the potential dependence of the in situ Raman in three different spectral regions during the charging process. The peaks associated with S_4^{2-}, S_4^-, $S_3^{\bullet-}$, and $S_2O_4^{2-}$ grow during charging starting at ca. 2.0 V and disappear at ∼2.6 V. The S_8-associated peak is produced at 2.5 V charge process and reach a maximum at 2.6 V. Figure 4D shows the potential dependence of the peak intensities associated with S_4^-, S_4^{2-}, $S_3^{\bullet-}$, $S_2O_4^{2-}$, and S_8. All peak intensities were normalized to the intense 534 cm^{-1} peak at 2.3 V. Correspondence with the CV shows that the oxidation peak at ∼2.4 V and the small shoulder at ∼2.25 V are associated with the formation of short-chain polysulfides during the anodic scan. This result shows that the

DOI: 10.1021/am5072942
ACS Appl. Mater. Interfaces 2015, 7, 1709−1719

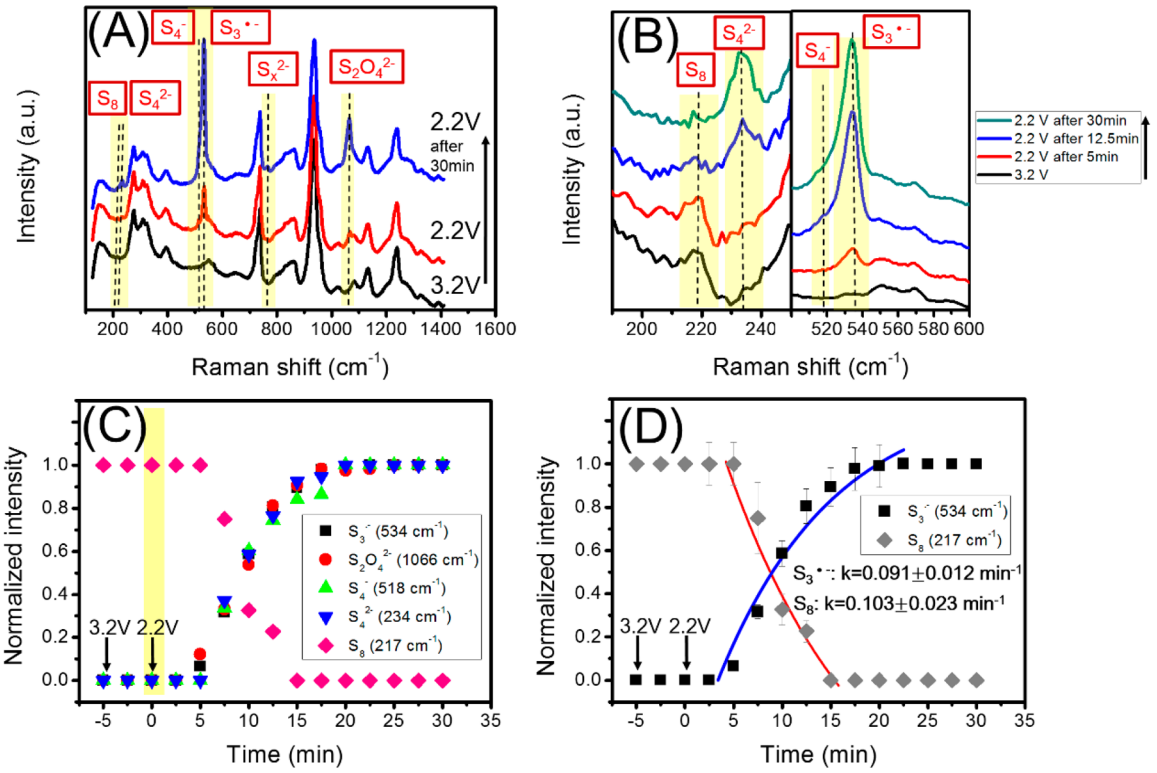

Figure 5. (A) In situ Raman spectra of the sulfur−carbon cathode obtained during discharge from 3.2 to 2.2 V and after holding the potential at 2.2 V for 30 min. (B) In situ Raman spectra at 180−250 and 500−600 cm^{-1} regions taken from 3.2 and 2.2 V during partial discharge. (C) Normalized intensity of S_8 and short-chain polysulfides species were plotted as a function of time after switching the potential from 3.2 to 2.2 V. (D) Fitting profiles for S_8 decomposition and the formation of short-chain polysulfides species.

different short-chain polysulfides are oxidized between 2.4 to 2.6 V. Long-chain polysulfides or S_8 are first observed at 2.5 V, showing that the oxidation peak at ∼2.5 V is associated with the formation of long-chain polysulfides and S_8. This result shows that the S_8 is reformed during the charge process, which is expected.[6,11,12]

3.4. Kinetics of Polysulfide Formation during Discharge. In order to characterize the persistence of the different polysulfide species during a potential hold during discharge, we examined the Raman spectrum obtained during partial discharge of the slurry cathode. Figure 5A shows in situ Raman spectra of the sulfur−carbon cathode obtained at potentials between 3.2 and 2.2 V and that obtained after holding the potential at 2.2 V for 30 min. As expected, short-chain polysulfides such as S_4^{2-}, S_4^-, $S_3^{\bullet-}$, S_x^{2-} (x = 4−8), and $S_2O_4^{2-}$ are observed at 2.2 V. The intensity of peaks associated with these short-chain polysulfides grows at 2.2 V with time as shown in Figure 5B. Figure 5C shows the normalized intensity of the Raman bands associated with short-chain polysulfides plotted as a function of time after stepping the potential from 3.2 to 2.2 V. The intensity of the 534 cm^{-1} band reached a maximum ca. 20 min after the potential was switched to 2.2 V and did not diminish for the remaining 10 min of the measurement. This behavior shows that the polysulfide formed at this potential is stable under potential control, at least over this time scale.

The short-chain polysulfide could result from the reaction of $Li^+ + S_8 + e^- \rightarrow$ short-chain polysulfides. The high concentration of Li salt (1 M) was used to increase the conductivity in the electrochemistry system.[50−53] Thus, we can assume the Li^+ concentration remains constant during the reaction. A pseudo first-order fit was used to model the reaction kinetics for both short-chain polysulfide formation and S_8 decomposition. Figure 5D shows fits to an exponential function of the time-dependent change in intensity of peaks associated with the formation of short-chain polysulfides. The appearance of $S_3^{\bullet-}$ occurs with a rate constant k_f = 0.091 ± 0.012 min^{-1}. Figure 5D also shows an exponential fit to the time-dependent disappearance of S_8 following the potential step. In this case, S_8 disappears with a rate constant k_d = 0.103 ± 0.023 min^{-1}. The close correspondence between k_f and k_d show that the short-chain polysulfides are directly formed from S_8 decomposition. The close correspondence between k_f values for the different short-chain polysulfide species also suggests that the S_8 ring is cleaved randomly by Li.

3.5. Kinetics of Polysulfide Decomposition during Charge. Figure 6A shows in situ Raman spectra of the sulfur−carbon cathode obtained at potentials between 2.2 and 3.2 V and that obtained after holding the potential at 3.2 V for 120 min during charging. The short-chain polysulfides observed at 2.2 V were reduced at 3.2 V, which is expected. After switching the potential from 2.2 to 3.2 V, the intensity of peaks associated with S_8 increases and the intensity of peaks associated with short-chain polysulfides decreases with time as shown in Figure 6B. Finally, only the S_8 peak can be observed. Figure 6C shows the normalized intensity of the Raman bands associated with short-chain polysulfides plotted as a function of time after switching the potential from 2.2 to 3.2 V. The intensity of short-chain polysulfides decreases with time and disappears 30 min after the potential was switched to 3.2 V. Figure 6D shows the fitting profiles to the decomposition of short-chain polysulfides and the formation of S_8. The rate constant is $k_{d'}$

DOI: 10.1021/am5072942
ACS Appl. Mater. Interfaces 2015, 7, 1709−1719

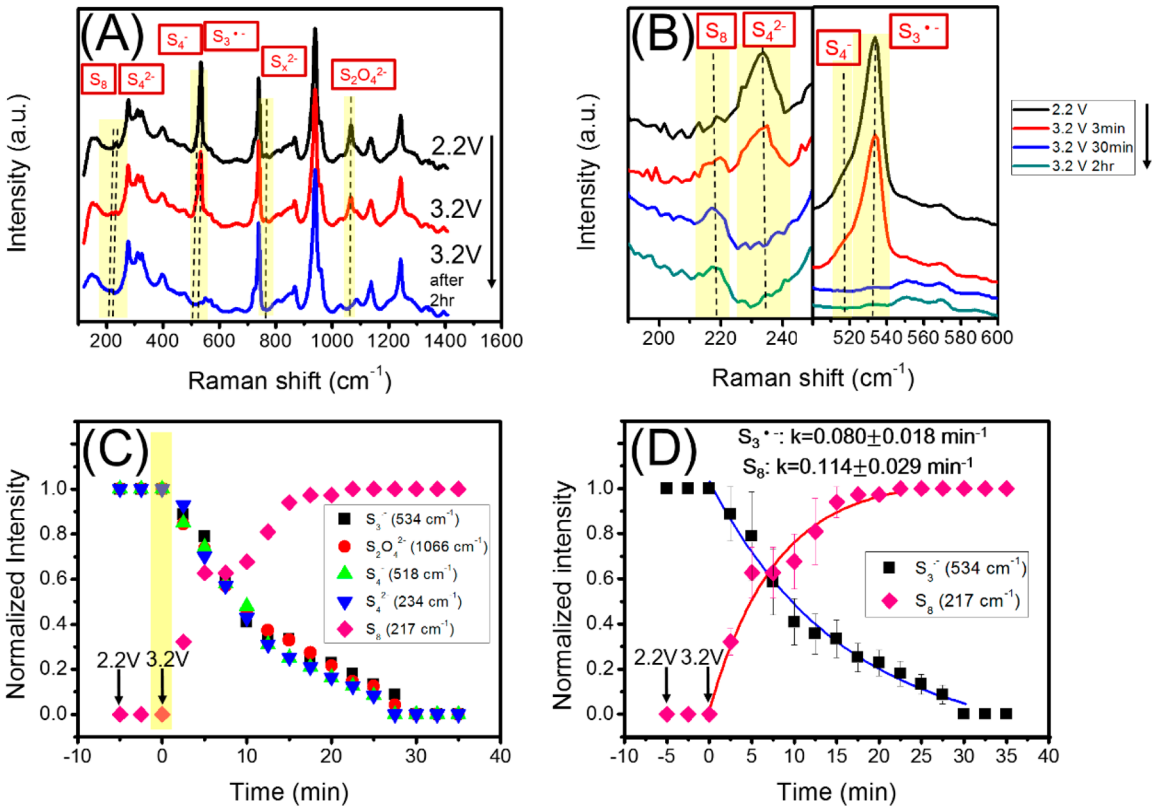

Figure 6. (A) In situ Raman spectra of the sulfur−carbon cathode obtained during charge from 2.2 to 3.2 V and after holding the potential at 3.2 V for 120 min. (B) In situ Raman spectra at 180−250 cm^{-1} and 500−600 cm^{-1} regions taken from 2.2 and 3.2 V during partial discharge. (C) Normalized intensity of S_8 and short-chain polysulfides species were plotted as a function of time after switching the potential from 2.2 to 3.2 V. (D) Fitting profiles for S_8 decomposition and the formation of short-chain polysulfides species.

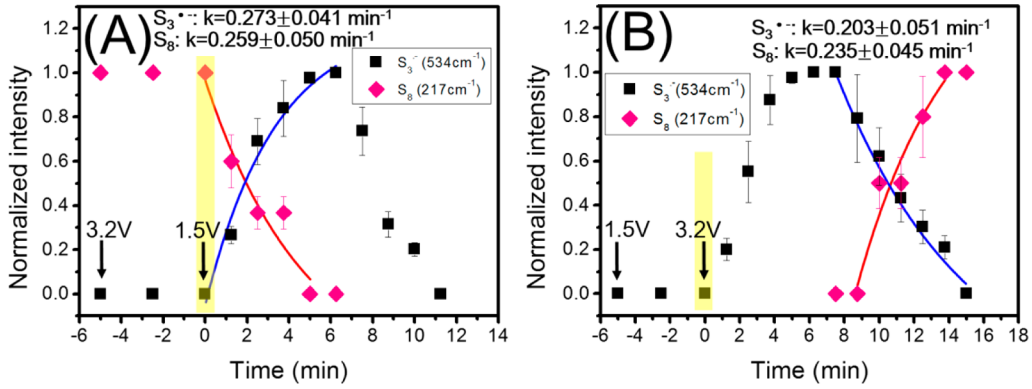

Figure 7. Normalized intensity of S_8 and short-chain polysulfides ($S_3^{\bullet-}$) were plotted as a function of time after switching the potential from (A) 3.2 to 1.5 V (discharge process) and (B) 1.5 to 3.2 V (charge process).

= 0.080 ± 0.018 min^{-1} for the decomposition of $S_3^{\bullet-}$ and k_f = 0.114 ± 0.029 min^{-1} for the formation of S_8. The rate constants for charge and discharge are thus similar to each other, suggesting that polysulfide oxidation and reduction is quasi-reversible.

We next examine the rate constants for full charge and discharge of the sulfur slurry cathode. Figure 7 shows the normalized intensity of the band associated with S_8 and those associated with $S_3^{\bullet-}$ plotted as a function of time after switching the potential from (A) 3.2 to 1.5 V during the discharge process and (B) 1.5 to 3.2 V during the charge process. During the discharge process from 3.2 to 1.5 V (Figure 7A), the intensity of the peak associated with $S_3^{\bullet-}$ grows with time and reach a maximum after 6 min. S_8 is initially present, but disappears after ∼6 min. After 6 min, the intensity associated with $S_3^{\bullet-}$ starts to decrease and disappears at 11.25 min, suggesting the decomposition of $S_3^{\bullet-}$ and the formation of Li_2S.

Figure 7A shows an exponential fit to the time-dependent disappearance of S_8 and appearance of $S_3^{\bullet-}$ following the potential step. S_8 disappears with a rate constant k_d = 0.259 ± 0.050 min^{-1} and $S_3^{\bullet-}$ appears with a rate constant k_f = 0.273 ± 0.041 min^{-1}. The close correspondence between k_f and k_d show that the short-chain polysulfides are directly formed from S_8 decomposition. The k values obtained following a step to 1.5 V are 2−3 fold larger than that obtained following at step 2.2 V

DOI: 10.1021/am5072942
ACS Appl. Mater. Interfaces 2015, 7, 1709−1719

(Figures 5 and 6) which is a consequence of the greater driving force to decompose S_8 and form $S_3^{\bullet-}$. As expected, Figure 7B shows that $S_3^{\bullet-}$ grows after switching the potential from 1.5 to 3.2 V. The peak intensity associated with $S_3^{\bullet-}$ reaches a maximum after 6 min. After 6 min, the decrease of $S_3^{\bullet-}$-associated peak intensity corresponds to the increase of S_8-associated peak intensity, suggesting the formation of short-chain polysulfides such as $S_3^{\bullet-}$ is followed by S_8 formation during the charge process. The apparent rate constants found during charging are similar to those obtained during discharge.

3.6. Changing Reactivity with CS_2 Addition. The analysis described above shows that S_8 decomposition occurs stepwise, via formation of progressively shorter-chain polysulfides as the potential is made more negative. We wondered whether we could control the stepwise decomposition of S_8 through a solution additive such as CS_2. Li cations in solution terminate the ends of the polysulfides as the polysulfide chain becomes shorter in a manner analogous to an organolithium reagent. Organolithium (RLi) contain very polar carbon−metal bonds. Thus, they are very reactive reagents. These organolithium reagents are widely used to add organic groups to substrates via nucleophilic addition or simple deprotonation.[54]

Organolithium reagents can also react with carbon dioxide to form carboxylic acids.[55] CS_2 reacts with organolithium complexes to make thiocarbonyl compounds or accumulate thiocarbonyl groups in the addition reaction of thiocarbonyl compounds. CS_2 is also used to react with organolithium reagents such as 1,4-dilithio-1,3-diene derivatives via carbophilic addition and thiophilic addition to generate thiophenes.[56,57]

Figure 8 shows CV obtained between 3.2 and 1.9 V from the as-prepared sulfur−carbon cathode at a scan rate of 0.5 mV/s

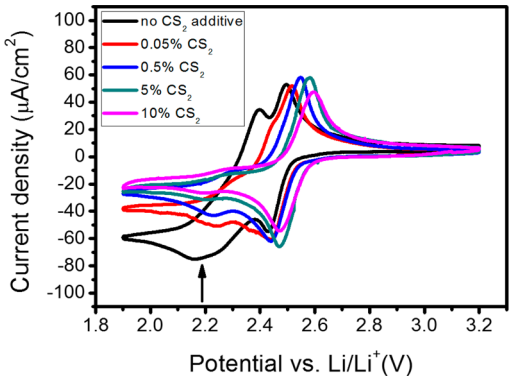

Figure 8. Cyclic voltammetry of the as-prepared sulfur−carbon cathode at a scan rate of 0.5 mV/s with different amounts of carbon disulfide (CS_2) (by vol.).

with addition of different amounts of CS_2 (by vol). CS_2 forms carbon polysulfides such as CS_3^{2-} and CS_4^{2-} in the region between 1.9 to 1.5 V.[58,59] The CV shows that the second reduction peak at ∼2.2 V (denoted by the arrow) decreases with increasing amounts of CS_2 and only one reduction peak is found after addition of 5% CS_2. The oxidative peak also shifts to positive potential from 2.5 to 2.6 V.

Figure 9A, B shows Raman spectra of the sulfur−carbon cathode obtained during discharge with addition of (A) 0.5% CS_2 and (B) 10% CS_2. The intensity of the C−S peaks (stretching mode) at 666 and 800 cm^{-1} varies with the amounts of CS_2 as shown in the Supporting Information (Figure S3).[60,61] During discharge in 0.5% CS_2, peaks associated with $S_3^{\bullet-}$ and S_4^{-} grow at 2.4 V after the decomposition of S_8 as shown in Figure 9A. However, the intensity of the bands associated with these species is very low compared with that in Figure 3 where CS_2 was absent. Figure S4 in the Supporting Information shows that the relative intensity of the peak associated with $S_3^{\bullet-}$ decreases with the amount of added CS_2. With addition of 10% CS_2 (Figure 9B), no peaks associated with $S_3^{\bullet-}$ formation were observed during discharge. However, the S_8 peak is persistent, which suggests the CS_2 additive does not affect S_8 at OCP. Figure 9C, D shows the CV of the as-prepared sulfur−carbon cathode in (C) 0.5% CS_2 and (D) 10% CS_2 along with the potential dependence of the peak intensities at 217 cm^{-1} (S_8) and 534 cm^{-1} ($S_3^{\bullet-}$) taken from A and B, respectively. The Raman intensities in Figure 9C were normalized to the 534 cm^{-1} peak at 2.2 V during discharge process. The intensity of the $S_3^{\bullet-}$ peak is very low in 0.5% CS_2. CV data in Figure 9C shows the second reduction peak around 2.2 V has little intensity, which is in a good agreement with the Raman data. The CV in Figure 9D shows only one reduction peak around 2.5 V in 10% CS_2. The Raman data shows only S_8 decomposition in the first reduction peak. Although carbon polysulfides such as CS_3^{2-} and CS_4^{2-} can be formed in the region of 1.9 to 1.5 V, no other polysulfides were observed before 1.9 V during discharge process. Thus, formation of short-chain polysulfides is suppressed by CS_2. CS_2 addition poisons the sulfur−carbon cathode and inhibits the reduction of long-chain polysulfides.

Figure 10 shows a possible explanation for the behavior observed with CS_2 addition. As illustrated in the Figure, S_8 is cleaved by Li^+ ion and forms S_8^{2-} in the first reduction peak. Short-chain polysulfides such as S_4^{2-} and $S_3^{\bullet-}$ form during further discharge as shown in pathway (a). Li_2S is the final product of discharge. Addition of CS_2 (pathway (b)) does not affect the formation of S_8^{2-} in the first reduction step. After the formation of long-chain lithium polyulfides, CS_2 will react with the lithium polysulfides to form stable compounds. Thus, the long-chain lithium polysulfides cannot be further reduced to short-chain polysulfides before 1.9 V.

4. CONCLUSIONS

In situ Raman and CV experiments clearly confirm that various lithium polysulfides are formed in two steps during discharge, including long-chain polysulfides (S_8^{2-}) and short-chain polysulfides such as S_4^{2-}, S_4^{-}, $S_3^{\bullet-}$, and $S_2O_4^{2-}$. The S_8 ring opening results in the formation of long-chain polysulfides at ∼2.4 V and the short-chain polysulfides appear at ∼2.3 V. These short-chain polysulfides decompose again at 1.6 V. During charge process, polysulfides and S_8 were reformed sequentially in different potential regions. Rate constants obtained by fitting the appearance and disappearance of bands to a pseudo first order reaction show that S_8 disappearance and polysulfide appearance occur at approximately the same rate, a rate that is similar whether the electrode is being charged or discharged.

CS_2 addition was used to change the sulfur reduction mechanism. While long-chain polysulfides are formed in the first reduction peak, CS_2 addition inhibits the appearance of further discharge products, ostensibly by stabilizing the long-chain polysulfide. The S_8^{2-} stabilization found here suggests that other additives might be successful in stabilizing other Li−S battery discharge products.

DOI: 10.1021/am5072942
ACS Appl. Mater. Interfaces 2015, 7, 1709−1719

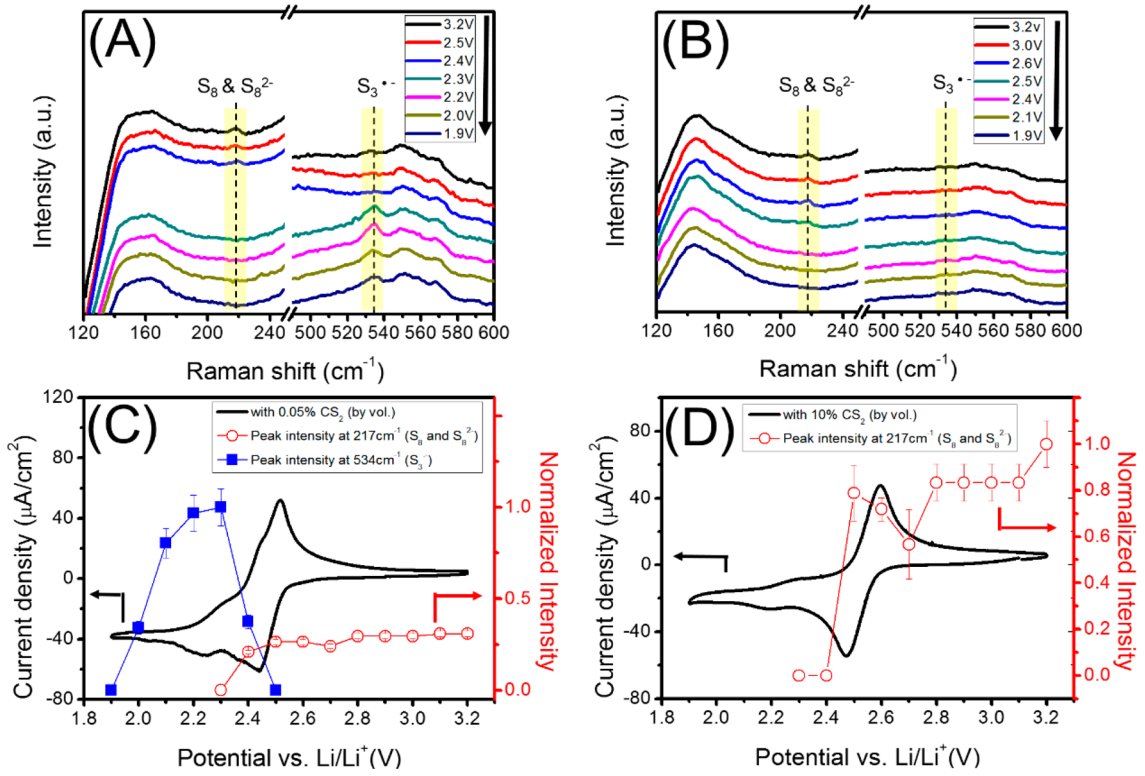

Figure 9. In situ Raman spectra of sulfur−carbon cathode obtained during discharge with (A) 0.5% CS_2 additive and (B) 10% CS_2 additive (by vol). Cyclic voltammetry of the as-prepared sulfur−carbon cathode in (C) 0.5% CS_2 and (D) 10% CS_2 with potential dependence of the peak intensities at 217 cm^{-1} (S_8) and 534 cm^{-1} ($S_3^{\bullet-}$) taken from A and B, respectively.

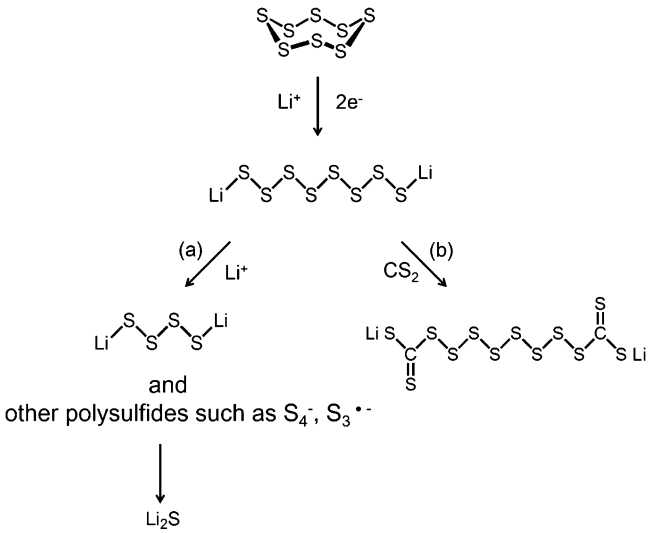

Figure 10. Schematic drawing of the sulfur reduction pathway (a) without and (b) with CS_2.

■ ASSOCIATED CONTENT

Supporting Information

Cyclic voltammetry of the sulfur−carbon cathode at a scan rate of 20 μV/s in coin cell (Figure S1). In- situ Raman spectra of the sulfur−carbon cathode shown at 3.2 V in 1 M LiTFSI with TEGDME/DIOX (1:1, by vol) (Figure S2). Vibrational frequencies and assignments of TFSI-, TEGDME, and DIOX for the Raman spectrum as shown in Figure S2 (Table S1). In situ Raman spectra of sulfur−carbon cathode obtained during discharge with (A) 0.5% CS_2 additive and (B) 10% CS_2 additive (by vol) at 3.2 V (Figure S3). The ratio of maximum peak intensity for $S_3^{\bullet-}$ (534 cm^{-1}) and C−O−C bending mode of 1,3-dioxolane (727 cm^{-1}) were plotted as a function of different amounts of CS_2 (Figure S4). This material is available free of charge via the Internet at http://pubs.acs.org."

■ AUTHOR INFORMATION

Corresponding Author

* E-mail: agewirth@illinois.edu. Tel: 217-333-8329. Fax: 217-244-5186.

Notes

The authors declare no competing financial interest.

■ ACKNOWLEDGMENTS

This work was supported as part of the Joint Center for Energy Storage Research (JCESR), an Energy Innovation Hub funded by the U.S. Department of Energy, Office of Science, Basic Energy Sciences.

■ REFERENCES

(1) Bruce, P. G.; Freunberger, S. A.; Hardwick, L. J.; Tarascon, J.-M. Li-O2 and Li-S batteries with high energy storage. *Nat. Mater.* **2012**, *11*, 19−29.

(2) Ji, X.; Nazar, L. F. Advances in Li-S batteries. *J. Mater. Chem.* **2010**, *20*, 9821−9826.

(3) Zhang, S. S. Liquid electrolyte lithium/sulfur battery: Fundamental chemistry, problems, and solutions. *J. Power Sources* **2013**, *231*, 153−162.

(4) Wang, D.-W.; Zeng, Q.; Zhou, G.; Yin, L.; Li, F.; Cheng, H.-M.; Gentle, I. R.; Lu, G. Q. M. Carbon-sulfur composites for Li-S batteries: status and prospects. *J. Mater. Chem. A* **2013**, *1*, 9382−9394.

DOI: 10.1021/am5072942
ACS Appl. Mater. Interfaces 2015, 7, 1709−1719

(5) Evers, S.; Nazar, L. F. New Approaches for High Energy Density Lithium−Sulfur Battery Cathodes. *Acc. Chem. Res.* **2012**, *46*, 1135−1143.
(6) Yeon, J.-T.; Jang, J.-Y.; Han, J.-G.; Cho, J.; Lee, K. T.; Choi, N.-S. Raman Spectroscopic and X-ray Diffraction Studies of Sulfur Composite Electrodes during Discharge and Charge. *J. Electrochem. Soc.* **2012**, *159*, A1308−A1314.
(7) Hagen, M.; Schiffels, P.; Hammer, M.; Dörfler, S.; Tübke, J.; Hoffmann, M. J.; Althues, H.; Kaskel, S. In-Situ Raman Investigation of Polysulfide Formation in Li-S Cells. *J. Electrochem. Soc.* **2013**, *160*, A1205−A1214.
(8) Barchasz, C.; Molton, F.; Duboc, C.; Leprêtre, J.-C.; Patoux, S.; Alloin, F. Lithium/Sulfur Cell Discharge Mechanism: An Original Approach for Intermediate Species Identification. *Anal. Chem.* **2012**, *84*, 3973−3980.
(9) Patel, M. U. M.; Demir-Cakan, R.; Morcrette, M.; Tarascon, J.-M.; Gaberscek, M.; Dominko, R. Li-S Battery Analyzed by UV/Vis in Operando Mode. *ChemSusChem* **2013**, *6*, 1177−1181.
(10) Cuisinier, M.; Cabelguen, P.-E.; Evers, S.; He, G.; Kolbeck, M.; Garsuch, A.; Bolin, T.; Balasubramanian, M.; Nazar, L. F. Sulfur Speciation in Li−S Batteries Determined by Operando X-ray Absorption Spectroscopy. *J. Phys. Chem. Lett.* **2013**, *4*, 3227−3232.
(11) Nelson, J.; Misra, S.; Yang, Y.; Jackson, A.; Liu, Y.; Wang, H.; Dai, H.; Andrews, J. C.; Cui, Y.; Toney, M. F. In Operando X-ray Diffraction and Transmission X-ray Microscopy of Lithium Sulfur Batteries. *J. Am. Chem. Soc.* **2012**, *134*, 6337−6343.
(12) Walus, S.; Barchasz, C.; Colin, J.-F.; Martin, J.-F.; Elkaim, E.; Lepretre, J.-C.; Alloin, F. New insight into the working mechanism of lithium-sulfur batteries: in situ and operando X-ray diffraction characterization. *Chem. Commun.* **2013**, *49*, 7899−7901.
(13) Su, Y.-S.; Fu, Y.; Cochell, T.; Manthiram, A. A strategic approach to recharging lithium-sulphur batteries for long cycle life. *Nat. Commun.* **2013**, *4*.
(14) Yamin, H.; Gorenshtein, A.; Penciner, J.; Sternberg, Y.; Peled, E. Lithium Sulfur Battery: Oxidation/Reduction Mechanisms of Polysulfides in THF Solutions. *J. Electrochem. Soc.* **1988**, *135*, 1045−1048.
(15) Martin, R. P.; Doub, W. H.; Roberts, J. L.; Sawyer, D. T. Electrochemical reduction of sulfur in aprotic solvents. *Inorg. Chem.* **1973**, *12*, 1921−1925.
(16) Merritt, M. V.; Sawyer, D. T. Electrochemical reduction of elemental sulfur in aprotic solvents. Formation of a stable S8- species. *Inorg. Chem.* **1970**, *9*, 211−215.
(17) Kim, B. S.; Park, S. M. In Situ Spectroelectrochemical Studies on the Reduction of Sulfur in Dimethyl Sulfoxide Solutions. *J. Electrochem. Soc.* **1993**, *140*, 115−122.
(18) Gaillard, F.; Levillain, E. Visible time-resolved spectroelectrochemistry: application to study of the reduction of sulfur (S8) in dimethylformamide. *J. Electroanal. Chem.* **1995**, *398*, 77−87.
(19) Han, D.-H.; Kim, B.-S.; Choi, S.-J.; Jung, Y.; Kwak, J.; Park, S.-M. Time-Resolved In Situ Spectroelectrochemical Study on Reduction of Sulfur in N, N′-Dimethylformamide. *J. Electrochem. Soc.* **2004**, *151*, E283−E290.
(20) Manan, N. S. A.; Aldous, L.; Alias, Y.; Murray, P.; Yellowlees, L. J.; Lagunas, M. C.; Hardacre, C. Electrochemistry of Sulfur and Polysulfides in Ionic Liquids. *J. Phys. Chem. B* **2011**, *115*, 13873−13879.
(21) Huff, L. A.; Rapp, J. L.; Baughman, J. A.; Rinaldi, P. L.; Gewirth, A. A. Identification of lithium−sulfur battery discharge products through 6Li and 33S solid-state MAS and 7Li solution NMR spectroscopy. *Surf. Sci.* **2015**, *631*, 295−300.
(22) Diao, Y.; Xie, K.; Xiong, S.; Hong, X. Insights into Li-S Battery Cathode Capacity Fading Mechanisms: Irreversible Oxidation of Active Mass during Cycling. *J. Electrochem. Soc.* **2012**, *159*, A1816−A1821.
(23) Simmonds, A. G.; Griebel, J. J.; Park, J.; Kim, K. R.; Chung, W. J.; Oleshko, V. P.; Kim, J.; Kim, E. T.; Glass, R. S.; Soles, C. L.; Sung, Y.-E.; Char, K.; Pyun, J. Inverse Vulcanization of Elemental Sulfur to Prepare Polymeric Electrode Materials for Li−S Batteries. *ACS Macro Lett.* **2014**, *3*, 229−232.
(24) Xiong, S.; Xie, K.; Diao, Y.; Hong, X. Oxidation process of polysulfides in charge process for lithium−sulfur batteries. *Ionics* **2012**, *18*, 867−872.
(25) Long, B. R.; Chan, M. K. Y.; Greeley, J. P.; Gewirth, A. A. Dopant Modulated Li Insertion in Si for Battery Anodes: Theory and Experiment. *J. Phys. Chem. C* **2011**, *115*, 18916−18921.
(26) Aggarwal, R. L.; Farrar, L. W.; Polla, D. L. Measurement of the absolute Raman scattering cross sections of sulfur and the standoff Raman detection of a 6-mm-thick sulfur specimen at 1500 m. *J. Raman Spectrosc.* **2011**, *42*, 461−464.
(27) Nimon, L. A.; Neff, V. D.; Cantley, R. E.; Buttlar, R. O. The infrared and Raman spectra of S6. *J. Mol. Spectrosc.* **1967**, *22*, 105−108.
(28) Dubois, P.; Lelieur, J. P.; Lepoutre, G. Identification and characterization of lithium polysulfides in solution in liquid ammonia. *Inorg. Chem.* **1988**, *27*, 73−80.
(29) Janz, G. J.; Coutts, J. W.; Downey, J. R.; Roduner, E. Raman studies of sulfur-containing anions in inorganic polysulfides. Potassium polysulfides. *Inorg. Chem.* **1976**, *15*, 1755−1759.
(30) Daly, F. P.; Brown, C. W. Raman spectra of sulfur dissolved in primary amines. *J. Phys. Chem.* **1973**, *77*, 1859−1861.
(31) Janz, G. J.; Roduner, E.; Coutts, J. W.; Downey, J. R. Raman studies of sulfur-containing anions in inorganic polysulfides. Barium trisulfide. *Inorg. Chem.* **1976**, *15*, 1751−1754.
(32) El Jaroudi, O.; Picquenard, E.; Gobeltz, N.; Demortier, A.; Corset, J. Raman Spectroscopy Study of the Reaction between Sodium Sulfide or Disulfide and Sulfur: Identity of the Species Formed in Solid and Liquid Phases. *Inorg. Chem.* **1999**, *38*, 2917−2923.
(33) El Jaroudi, O.; Picquenard, E.; Demortier, A.; Lelieur, J.-P.; Corset, J. Polysulfide Anions. 1. Structure and Vibrational Spectra of the S22- and S32- Anions. Influence of the Cations on Bond Length and Angle. *Inorg. Chem.* **1999**, *38*, 2394−2401.
(34) El Jaroudi, O.; Picquenard, E.; Demortier, A.; Lelieur, J.-P.; Corset, J. Polysulfide Anions II: Structure and Vibrational Spectra of the S42- and S52- Anions. Influence of the Cations on Bond Length, Valence, and Torsion Angle. *Inorg. Chem.* **2000**, *39*, 2593−2603.
(35) Janz, G. J.; Downey, J. R.; Roduner, E.; Wasilczyk, G. J.; Coutts, J. W.; Eluard, A. Raman studies of sulfur-containing anions in inorganic polysulfides. Sodium polysulfides. *Inorg. Chem.* **1976**, *15*, 1759−1763.
(36) Clark, R. J. H.; Cobbold, D. G. Characterization of sulfur radical anions in solutions of alkali polysulfides in dimethylformamide and hexamethylphosphoramide and in the solid state in ultramarine blue, green, and red. *Inorg. Chem.* **1978**, *17*, 3169−3174.
(37) Daly, F. P.; Brown, C. W. Raman spectra of sodium tetrasulfide in primary amines. Evidence for sulfide (S42- and S8n-) ions in rhombic sulfur-amine solutions. *J. Phys. Chem.* **1975**, *79*, 350−354.
(38) Chivers, T.; Lau, C. Raman spectroscopic identification of the S4N- and S3- ions in blue solutions of sulfur in liquid ammonia. *Inorg. Chem.* **1982**, *21*, 453−455.
(39) Khan, S. A.; Hughes, R. W.; Reynolds, P. A. Raman spectroscopic determination of oxoanions in aqueous polysulfide electrolyte solutions. *Vib. Spectrosc.* **2011**, *56*, 241−244.
(40) Wang, J.; Chen, J.; Konstantinov, K.; Zhao, L.; Ng, S. H.; Wang, G. X.; Guo, Z. P.; Liu, H. K. Sulphur-polypyrrole composite positive electrode materials for rechargeable lithium batteries. *Electrochim. Acta* **2006**, *51*, 4634−4638.
(41) Yu, X.-g.; Xie, J.-y.; Yang, J.; Huang, H.-j.; Wang, K.; Wen, Z.-s. Lithium storage in conductive sulfur-containing polymers. *J. Electroanal. Chem.* **2004**, *573*, 121−128.
(42) Chivers, T. Ubiquitous trisulphur radical ion S3-. *Nature* **1974**, *252*, 32−33.
(43) Chivers, T.; Elder, P. J. W. Ubiquitous trisulfur radical anion: fundamentals and applications in materials science, electrochemistry, analytical chemistry and geochemistry. *Chem. Soc. Rev.* **2013**, *42*, 5996−6005.
(44) Vijayakumar, M.; Govind, N.; Walter, E.; Burton, S. D.; Shukla, A.; Devaraj, A.; Xiao, J.; Liu, J.; Wang, C.; Karim, A.; Thevuthasan, S. Molecular structure and stability of dissolved lithium polysulfide species. *Phys. Chem. Chem. Phys.* **2014**, *16*, 10923−10932.

DOI: 10.1021/am5072942
ACS Appl. Mater. Interfaces 2015, 7, 1709−1719

(45) Chivers, T.; Drummond, I. Characterization of the trisulfur radical anion S3- in blue solutions of alkali polysulfides in hexamethylphosphoramide. *Inorg. Chem.* **1972**, *11*, 2525−2527.
(46) Kim, H.; Jeong, T.-G.; Choi, N.-S.; Kim, Y.-T. The cycling performances of lithium−sulfur batteries in TEGDME/DOL containing LiNO3 additive. *Ionics* **2013**, *19*, 1795−1802.
(47) Takahashi, H.; Kaneko, N.; Miwa, K. Raman and infrared studies of the structure of the dithionite ion in aqueous solution and force-constants of S2Ox2− type ions. *Spectrochim. Acta, Part A* **1982**, *38*, 1147−1153.
(48) Diao, Y.; Xie, K.; Xiong, S.; Hong, X. Shuttle phenomenon − The irreversible oxidation mechanism of sulfur active material in Li−S battery. *J. Power Sources* **2013**, *235*, 181−186.
(49) Seo, I.; Martin, S. W. Structural Properties of Lithium Thio-Germanate Thin Film Electrolytes Grown by Radio Frequency Sputtering. *Inorg. Chem.* **2011**, *50*, 2143−2150.
(50) Lee, D.-J.; Agostini, M.; Park, J.-W.; Sun, Y.-K.; Hassoun, J.; Scrosati, B. Progress in Lithium−Sulfur Batteries: The Effective Role of a Polysulfide-Added Electrolyte as Buffer to Prevent Cathode Dissolution. *ChemSusChem* **2013**, *6*, 2245−2248.
(51) Yang, Y.; Zheng, G.; Cui, Y. A membrane-free lithium/polysulfide semi-liquid battery for large-scale energy storage. *Energy Environ. Sci.* **2013**, *6*, 1552−1558.
(52) Zhang, S. S.; Read, J. A. A new direction for the performance improvement of rechargeable lithium/sulfur batteries. *J. Power Sources* **2012**, *200*, 77−82.
(53) Agostini, M.; Lee, D.-J.; Scrosati, B.; Sun, Y. K.; Hassoun, J. Characteristics of Li2S8-tetraglyme catholyte in a semi-liquid lithium−sulfur battery. *J. Power Sources* **2014**, *265*, 14−19.
(54) Reich, H. J. Role of Organolithium Aggregates and Mixed Aggregates in Organolithium Mechanisms. *Chem. Rev.* **2013**, *113*, 7130−7178.
(55) Ronald, R. C. Methoxymethyl ethers. An activating group for rapid and regioselective metalation. *Tetrahedron Lett.* **1975**, *16*, 3973−3974.
(56) Chen, J.; Song, Q.; Xi, Z. Novel reaction patterns of carbon disulfide with organolithium compounds via cleavage of C═S bonds or via cycloaddition reactions. *Tetrahedron Lett.* **2002**, *43*, 3533−3535.
(57) Seyferth, D.; Hui, R. C. Reactions of in-situ generated acyllithium reagents with carbon disulfide and carbonyl sulfide. *Tetrahedron Lett.* **1984**, *25*, 2623−2626.
(58) Jeroschewski, P.; Pragst, F. Investigation on the mechanism of the electrochemical reduction of CS2 in aprotic solvents. *J. Electroanal. Chem. Interfacial Electrochem* **1983**, *149*, 131−137.
(59) Wawzonek, S.; Heilmann, S. M. Electrochemical reduction of carbon disulfide in dimethylformamide. *J. Org. Chem.* **1974**, *39*, 511−514.
(60) Langseth, A.; So/rensen, J. U.; Nielsen, J. R. Raman Spectrum of Carbon Disulphide. *J. Chem. Phys.* **1934**, *2*, 402−409.
(61) Ito, M. Raman and Infrared Spectra of Crystalline Carbon Disulfide. *J. Chem. Phys.* **1965**, *42*, 815−818.

DOI: 10.1021/am5072942
ACS Appl. Mater. Interfaces 2015, 7, 1709−1719